CrossMark

Comparison of spur, helical and curvilinear gear drives by means of stress and tooth contact analyses

Alfonso Fuentes-Aznar · Ramon Ruiz-Orzaez · Ignacio Gonzalez-Perez

Abstract Involute tooth surfaces are a successful technical solution for both spur and helical gear drives since they provide linear contact and a low-level function of transmission errors under good conditions of meshing. Tip relief is usually required to improve contact conditions during the transfer of meshing between adjacent pairs of teeth. Yet, unfavorable conditions of contact appear when shaft deflections and misalignments are present. Localization of contact through lead crowning is a solution that increases the cost of machining in both spur and helical gear drives. In this sense, the generation process of curvilinear gear drives provides localization of contact with no additional cost. Comparison of stresses and transmission error functions in spur, helical and curvilinear gear drives is investigated to show if the application of curvilinear gear drives yields some advantages respect to spur and helical gear drives. The three mentioned types of cylindrical parallel-axis gear drives are provided, firstly, with linear contact, and, secondly, with localized contact, for the purpose of comparison. Different misalignments conditions are taken into account by means of several numerical examples.

Keywords Curvilinear gears · Spur gears · Helical gears · Mechanical behavior · Stress analysis · Tooth contact analysis

1 Introduction

Involute spur and helical gear drives with parallel axes are widely used in reducers, planetary gear trains, gear pumps and many other industrial applications. Sophistication in the design and manufacture of such gears by hobbing, shaping and grinding procedures has reached an outstanding level.

Involute cylindrical gear sets are very sensitive to misalignments. Such errors lead to discontinuous linear functions of transmission errors, which result in vibration and noise as well as edge contacts, which simultaneously cause the appearance of areas of high contact stresses and the premature failure of the gear drive [15, 16]. Localization of bearing contact by crowning the active tooth surfaces in both profile and longitudinal directions of one of the mating gears is required.

A new type cylindrical parallel-axis gears with curvilinear shaped teeth, as well as their machining methods, was proposed almost a century ago [3], although it has been suggested that the first curved

A. Fuentes-Aznar (✉)
Department of Mechanical Engineering, Rochester Institute of Technology (RIT), Rochester, NY, USA
e-mail: afeme@rit.edu

R. Ruiz-Orzaez · I. Gonzalez-Perez
Department of Mechanical Engineering, Polytechnic University of Cartagena (UPCT), Cartagena, Spain
e-mail: rro0@alu.upct.es

I. Gonzalez-Perez
e-mail: ignacio.gonzalez@upct.es

tooth configuration was proposed in the first half of the nineteenth century [6]. This type of gear drive has received different denominations since it was proposed for the first time [6]. In this work, curvilinear gears has been the term employed.

The main advantage of curvilinear gears with regard to involute spur and helical gears is that the localization of bearing contact can be achieved in a simple generating process by using only a face-milling cutter and without applying double-crowning cutting procedures to the surfaces of one of the mating gears [11, 16]. Other benefits are also obtained as no axial thrust forces (similar to herringbone helical gear drives) during mechanical high power transmission, better lubrication conditions (oil retained within the concave tooth surface during operation) [21], and an inherent self-aligning capability [6].

Curvilinear gears were employed in the Chinese heavy industry (steel plants, aluminium rolling mills, or cement equipment plants) for the first time in 1980 [21]. In addition, Arafa [4, 5] proposed employing curvilinear gears provided with constant pressure angle in rotorcraft transmissions and wind turbine gearboxes instead of double-helical gears drives and planetary gear trains, respectively. Recently, Parshin [17] showed real applications of curvilinear gears in power transmissions.

Arafa [3, 6] was probably the first author in carrying out by far the most thorough review and classification of the different existing types of curvilinear gears, managing to distinguish between 11 types and, in turn, organizing them into two main groups: the first group comprises curvilinear gears with variable pressure angle along the tooth face width, called *CV-gears*, while the second group comprises curvilinear gears with constant pressure angle along the tooth face width, called *CC-gears*. The same author also showed the main advantages, disadvantages, and limitations of curvilinear gears. Because of the aforementioned reasons, the nomenclature of categorization of curvilinear gears proposed by Arafa will be employed in this work.

Virtual generation, undercutting conditions and contact characteristics of different types of curvilinear gears have been analysed in previous works. So, *CV1-gears* were analyzed in [21], *CV2-gears* in [22, 23], *CV3-gears* in [26], and *CC2-gears* in [2]. The same characteristics have been described in [24, 25], in which a new continuous indexing methodology of

manufacturing of curvilinear cylindrical gear drives by hob-cutters was proposed. In some previous works curvilinear gears have been compared with spur involute gears [18, 21] and helical involute gears [23].

This paper aims to achieve the following objectives:

1. Application of tooth contact and stress analyses to spur, helical and curvilinear gear drives for investigation of the evolution of contact and bending stresses along two cycles of meshing and the variation of the function of transmission errors (loaded and unloaded) by means of its peak-to-peak value. These analyses will provide a comparison of these gear drives from the point of view of their endurance and transmission errors as one of the sources of noise and vibration.
2. Comparison of spur, helical and curvilinear gear drives designed for linear contact under ideal assembly conditions. In this case, whereas spur and helical gear drives require only one generating process, curvilinear gear drives require the application of fixed-setting face-milling cutters for independent generation of convex and concave tooth sides.
3. Comparison of spur, helical and curvilinear gear drives designed for point contact under ideal assembly conditions. In this case, spur and helical gear drives requires an additional finishing process for longitudinal crowning whereas curvilinear gear drives require just one generating process by application of a spread-blade face-milling cutter.
4. Comparison of spur, helical and curvilinear gear drives manufactured with only one cutting process. In this case, spur and helical gear drives, produced by a rack-cutter or a hob, will show linear contact under ideal assembly conditions whereas curvilinear gear drives, produced by a spread-blade face-milled cutter, will show a localized bearing contact.
5. Optimization of tip relief for all cases of design in order to guarantee that spur, helical and curvilinear gear drives are free of areas with severe contact stresses at the top edge of the gear teeth under ideal assembly conditions.

Several numerical examples for comparison of spur, helical and curvilinear gear drives are presented. The

investigation considers either ideal assembly conditions or errors of alignment.

2 Generating processes and optimization of tip relief

In following Figs. 1, 2 and 3, the generating processes of spur, helical and curvilinear gears is represented. The following general coordinate systems are considered to represent the geometry of generated gears and generating tools:

- $S_g(x_g, y_g, z_g)$. This coordinate system is fixed to the being generated gear.
- $S_c(x_c, y_c, z_c)$. This coordinate system is fixed to the considered cutting or grinding tool. Its axis z_c is parallel to axis z_g of the generated gear.
- $S_t(x_t, y_t, z_t)$. This coordinate system is used to define the cross section of the generating tool. For spur and curvilinear gears, coordinate system S_t coincides with coordinate system S_c. Axis z_t is perpendicular to the cross section of the tool. Its origin O_t coincides with O_c, origin of the coordinate system S_c.
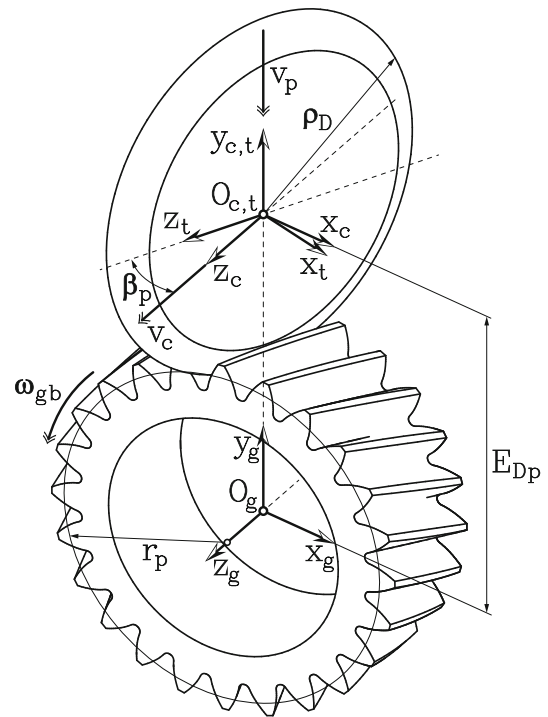

Fig. 2 Description of generating mechanism of helical cylindrical gears by plunging disk

2.1 Generation by rack-cutters

Generation of involute tooth surfaces in spur and helical gears by means of rack-cutters, or their equivalent hobs [15, 16, 19], is schematically illustrated in Fig. 1. Spur gears constitute a particular case of helical gears in which the helix angle is zero. During the generation process, the rack-cutter is translated with linear velocity v_c, along axis x_c and therefore perpendicular to the axis of rotation of the gear blank, whereas the gear blank is rotated with angular velocity ω_{gb} around axis z_g. The rack-cutter pitch plane remains tangent to gear pitch cylinder for standard tooth proportions when no profile shift is considered. Finally, the gear tooth surfaces are generated as the envelope to the family of positions of the rack-cutter tooth surfaces in its rolling without sliding relative motion over the gear pitch cylinder. The rolling without sliding condition is expressed mathematically through Eq. (1), where r_p is the pitch radius of the being-generated gear [15]. Additionally, during the generating process, the rack-cutter reciprocates with
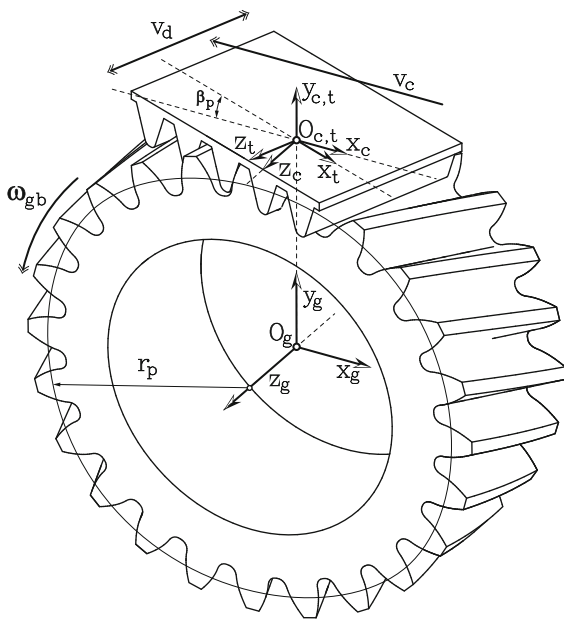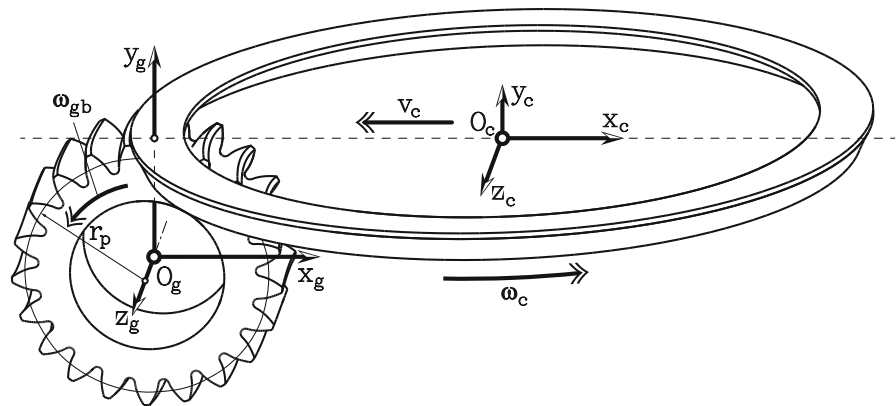

Fig. 1 Description of generating mechanism of helical cylindrical gears by a rack-cutter

Fig. 3 Description of generating mechanism of curvilinear cylindrical gears by face-milling cutter

cutting speed v_d (feed motion), which depends on the spur gear face width being generated [19] and has no effect on the generated geometry of the gear tooth surfaces from a theoretical point of view. The feed motion direction and the rotation axis of the gear blank form an angle equal to helix angle β_p. Generation by a rack-cutter (or a hob) allows spur and helical gears to be manufactured according to a single (or continuous) indexing process.

$$v_c = \omega_{gb} r_p \tag{1}$$

2.2 Generation by plunging disk

Generation by a plunging disk allows longitudinal crowning to be applied on both spur and helical gear tooth surfaces [15, 16]. The generation process is schematically illustrated in Fig. 2. The plunging disk performs screw and plunging motions relative to the gear being generated. The plunging disk is translated with linear velocity v_c along the rotation axis of the gear whereas the gear is rotated with angular velocity ω_{gb}. Both velocities are related with each other through Eq. (2). Additionally, plunging motion is performed with linear velocity v_p along the shortest distance direction between gear and grinding disk axes. Center distance E_{Dp} is modified according to Eq. (3). Here, a_{pl} is a parabola coefficient, ρ_D is the disk radius, b is the dedendum coefficient, m_n is the normal module, and ψ_1 is the angle of rotation of the gear. Grinding by a plunging disk allows spur and helical gears to be manufactured with a single indexing process. The mathematical model of longitudinal crowned gear tooth surfaces by application of a plunging disk has been already described in [15, 16].

$$v_c \tan \beta_p = \omega_{gb} r_p \tag{2}$$

$$E_{Dp} = \rho_D + (r_p - b m_n) - a_{pl} \left(\frac{r_p}{\tan \beta_p} \right)^2 \psi_1^2 \tag{3}$$

2.3 Generation by spread-blade face-milling cutter

In the present work, curvilinear cylindrical gears have been generated by means of face-milling cutters [11], as it is shown in Fig. 3. Basically, the generating procedure is similar to that described in Sect. 2.1, with the only difference that the rack-cutter is replaced by a face-milling cutter. Additionally, the face-milling cutter rotates around its own axis y_c with angular speed ω_c, which only affects the cutting or grinding velocity but has no effect on the obtained geometry of gear tooth surfaces from a theoretical point of view. The described cutting process constitutes a single indexing process.

The first type of curvilinear gear geometry analyzed in the present work is generated by a spread-blade face-milling cutter (SBC) comprising groups of pairs of alternating cutting or finishing blades: an outside blade and an inside blade. The resultant curvilinear gear drive has a localized bearing contact and variable pressure angle along the tooth face width. One of the most important features of this type of curvilinear gear is the relationship between the cutter mean pitch curvature radius r_c and the length of the mayor axis of the contact ellipses [23, 25, 26]. In addition, the relationships between the cutter mean pitch curvature radius, r_c, and the pitch curvature radii corresponding to the outside blades, r_{ob}, and the inside blades, r_{ib}, are

given by Eqs. (4). Figure 4 illustrates schematically a spread-blade face-milling cutter.

$$r_{ob} = r_c + \frac{\pi m_n}{4} \qquad (4a)$$

$$r_{ib} = r_c - \frac{\pi m_n}{4} \qquad (4b)$$

Curvilinear gears whose teeth have been generated by spread-blade face-milling cutters correspond to *CV2-gears*, according to Arafa's nomenclature [3, 6] and will be denoted here as *SBC-gears*.

2.4 Generation by fixed-setting face-milling cutters

The second type of curvilinear gear drive analyzed in the present work consists of a SBC gear member and a pinion member generated by a pair of fixed-setting face-milling cutters (FSC):

1. One fixed-setting cutter is comprised of outer cutting blades and is employed for generation of the concave side of the pinion tooth surfaces.
2. The other fixed-setting cutter is comprised of inner cutting blades and is employed for generation of the convex side of the pinion tooth surfaces.

Figure 5 shows a scheme of cross sections belonging to the previously described fixed-setting face-milling cutters. The corresponding relationships between the mean pitch curvature radius r_c of the gear member spread-blade cutter, and the pitch curvature radii of the the inner cutting blades, r_{ib}, and the outer cutting blades, r_{ob}, are given by Eqs. (4).

The resultant curvilinear gear drive has linear contact and variable pressure angle along the tooth face width. Essentially, they correspond to *CV3-gears*,

according to Arafa's nomenclature [3, 6] and will be denoted here as *FSC-gears*.

The mathematical model of curvilinear cylindrical gear tooth surfaces has already been described in depth in [11].

2.5 Optimization of tip relief

Tip relief consists of the continuously increasing removal of material on the top edge of the gear contacting surfaces which can be applied through linear or parabolic functions of deviations on the generating tool profile [13, 14]. When no tip relief is applied to the gear tooth active surfaces, areas of high contact stresses appear on the top edge of such surfaces. The application of an optimal degree of tip relief allows obtaining of a smooth evolution of contact stresses throughout the whole cycle of meshing and avoiding the appearance of areas of severe contact stresses. Consequently, maximum contact stresses are reduced drastically, and the endurance and life of gear transmissions are increased considerably. Tip relief modification increases slightly bending stresses because of the reduction of the effective contact ratio, which takes into account contacting tooth deformations.

In the present work, a parabolic tip relief will be introduced by modifying the cross section geometry of the generating tool. The tangency between the parabolic tip relief and the active generating profile impedes the appearance of edges on the gear tooth contacting surfaces, assuring a smoother load transition [10]. Figure 6 shows the geometry of the normal cross section of a generating rack-cutter. The same normal cross section as the one illustrated in Fig. 6 is considered for determination of the generating tools of a grinding disk and a face-milling cutter. In the case of a grinding disk, a reference gear tooth surface should be generated first for determination of a line of
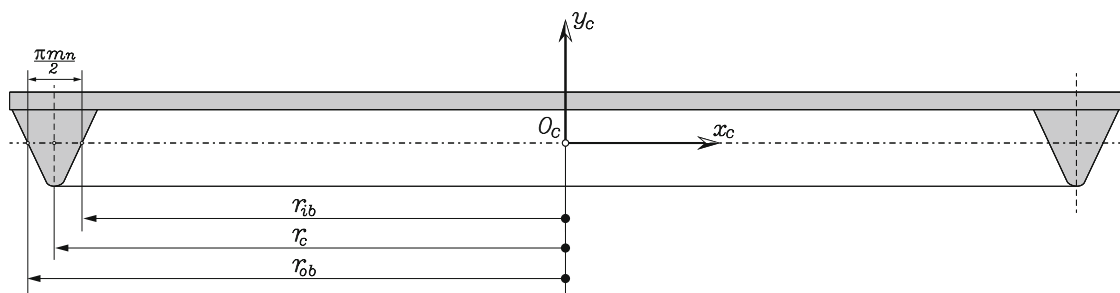

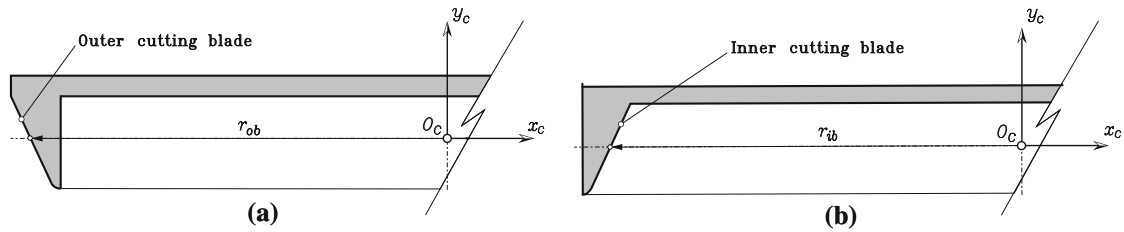**Fig. 4** Schematic representation of a spread-blade face-milling cutter cross section

Fig. 5 Schematic representation of cross section of a fixed-setting face-milling cutters with: **a** inner cutting blades, and **b** outer cutting blades
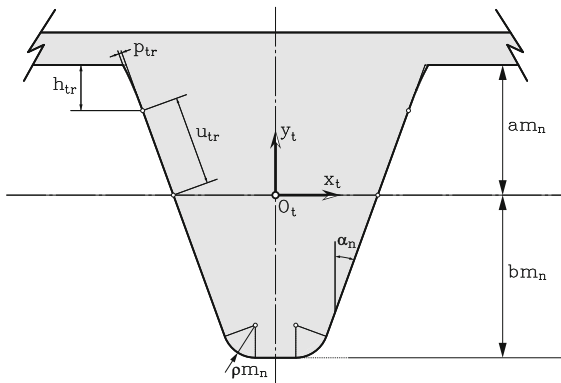

Fig. 6 Cross section of rack-cutter

tangency between the reference gear tooth surface and the sought-for disk surface [15, 16].

Parameter p_{tr} is the maximum deviation of parabolic tip relief and h_{tr} is a reference height for tip relief. Both parameters are related as

$$p_{tr} = a_{tr} \left(\frac{h_{tr}}{\cos \alpha_n} \right)^2 \tag{5}$$

where a_{tr} is the parabolic coefficient and α_n denotes the profile pressure angle in normal section. The value of profile parameter where tip relief starts, u_{tr}, is obtained from

$$h_{tr} = a \, m_n - u_{tr} \cos \alpha_n \tag{6}$$

Here, a is the addendum coefficient and m_n denotes the normal module.

3 Computerized simulation of gear meshing and tooth contact analysis

Computerized simulation of meshing and contact, directed to the determination of the contact pattern and

function of transmission errors, is based on the application of an enhanced algorithm for tooth contact analysis (TCA) and the application of a general purpose finite element analysis (FEA) computer program.

The proposed numerical approach constitutes a simulated loaded tooth contact analysis (SLTCA) technique [7], and it is based on the rigid body hypothesis of contact of mating surfaces; consequently, no elastic tooth deformation is taken into account for contact pattern determination. Basically, contact path tracing is based on the ideas presented in Sheveleva's work [20], according to which the relative position between pairs of contacting tooth surfaces is taken into account and the rotation of one of the member of the gear set is determined until contact is reached. Regarding contact pattern, it is computed by means of a purely geometric approach proposed in Bracci's work [8], according to which those points which are positioned a relative distance between surfaces in contact given by a virtual marking compound thickness, usually equal to 0.0065 mm, are considered to belong to contact ellipses. Finally, whereas unloaded transmission errors are obtained from the application of the mentioned algorithm for TCA, loaded transmission errors are derived as a particular procedure of the one proposed in [12], which is based on the application of a finite element analysis (FEA) computer program and will be described in detail in Sect. 4. Essentially, the described TCA algorithm is independent of the type of bearing contact between mating surfaces (point, line, or edge contact), does not require the solution of any system of nonlinear equations and takes into account the effect of adjacent pairs of meshing teeth on contact pattern.

The errors of alignment considered for simulation of meshing and contact are: (1) ΔA_2 as the axial displacement of the gear member with respect to the

pinion member, (2) ΔC as the center distance error, (3) ΔV as the intersecting shaft angle error, and (4) ΔH as the crossing shaft angle error.

3.1 Applied coordinate systems

The applied coordinate systems for TCA of any type of cylindrical gears are shown in Fig. 7. The following auxiliary coordinate systems have been defined:

- $S_f(x_f, y_f, z_f)$. This is the fixed coordinate system, attached rigidly to the gear transmission.
- $S_1(x_1, y_1, z_1)$. This movable coordinate system is attached to the pinion member of the gear transmission. Its corresponding rotation axis is z_1 and collinear with axis z_f of S_f coordinate system (Fig. 7a).
- $S_2(x_2, y_2, z_2)$. This movable coordinate system is attached to the gear member of the gear transmission. Its corresponding rotation axis is z_2 (Fig. 7b).
- $S_k(x_k, y_k, z_z)$. The three axes of this coordinate system are parallel to the ones of the fixed

coordinate system S_f, and its origin O_k is separated with respect to O_f a distance $C + \Delta C$ along axis y_f, where C denotes the transmission center distance (Fig. 7c).

- $S_l(x_l, y_l, z_l)$. The three axes of this coordinate system are parallel to the ones corresponding of coordinate system S_k, and its origin O_l is separated with respect to O_k a distance ΔA_2 along axis z_k (Fig. 7c).
- $S_m(x_m, y_m, z_m)$. This coordinate system allows the intersecting shaft angle error ΔV (Fig. 7c) to be simulated. Coordinate system S_m is rotated around axis x_m a magnitude ΔV with respect to coordinate system S_l.
- $S_n(x_n, y_n, z_n)$. This coordinate system allows the crossing shaft angle error ΔH (Fig. 7c) to be simulated. Coordinate system S_n is rotated around axis y_n a magnitude ΔH with respect to coordinate system S_m.

Angles $\phi^{(1)}$ and $\phi^{(2)}$ represent the angles of rotation of the pinion and gear members, respectively.

Fig. 7 Coordinate systems applied for simulation of meshing and contact
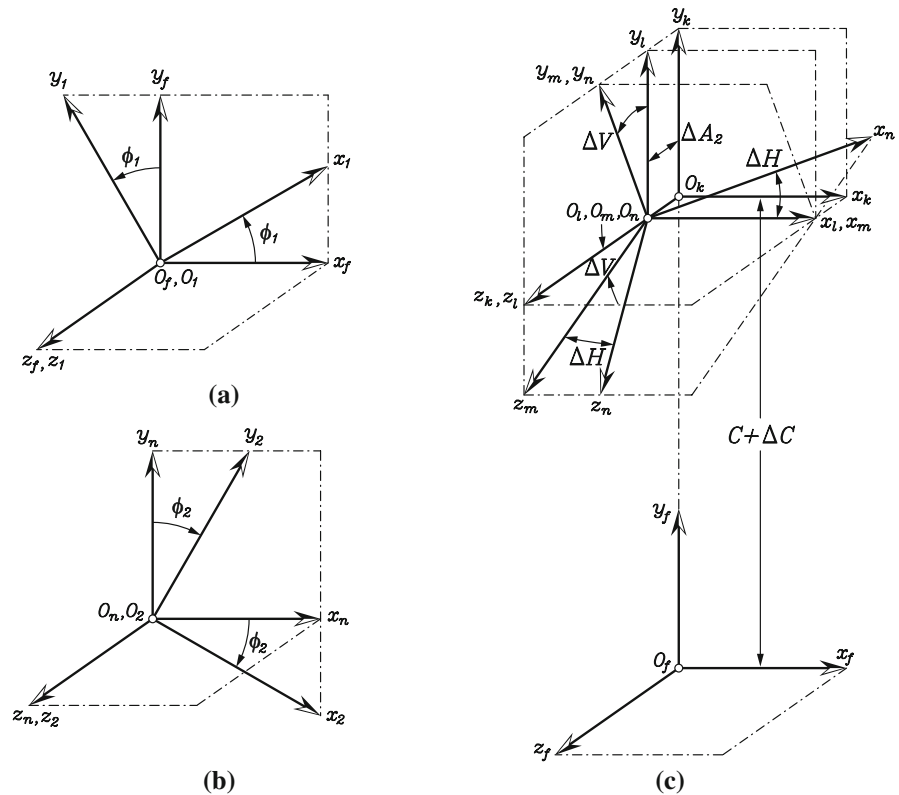
4 Stress analysis

The finite element method has been used to perform stress analysis of cylindrical gear drives. The evolution of contact and bending stresses throughout two cycles of meshing has been obtained, the formation of the bearing contact investigated, and areas of severe contact stress (edge contacts), if they exist, discovered. Automatic parametric generation of finite-element models of cylindrical gears has been carried out taking into account the ideas shown in [15, 16].

Finite element models comprising five pairs of contacting teeth have been employed to avoid influence of the boundary conditions on the results and to investigate the load sharing between pinion and wheel tooth surfaces. Figure 8 shows the finite element model of a cylindrical gear set. Gear active tooth surfaces have been defined as master surfaces, while pinion active tooth surfaces have been defined as slave surfaces. Three-dimensional solid elements of type C3D8I [1] have been used, being hexahedral first order elements enhanced by incompatible deformation modes in order to improve their bending behavior. Pinion and gear material is steel.

The total function of transmission errors will be derived according to a simplified procedure of the one proposed in [12]. Transmission errors are considered positive when the gear moves away from the pinion and negative when the gear approaches the pinion. The simplified procedure is as follows:

1. The function of unloaded transmission errors is obtained first as a discrete function:

$$\Delta\phi_i^{(u)} = \left(-\phi_i^{(2)} - \phi_i^{(1)}\frac{N_1}{N_2} \right) \tag{7}$$

   where $\phi_i^{(1)}$ and $\phi_i^{(2)}$ are the angular rotations that allows pinion and gear, respectively, to become in contact under no load at each contact position i. N_1 and N_2 are the tooth number of pinion and gear, respectively. $\phi_i^{(1)}$ and $\phi_i^{(2)}$ are obtained directly from TCA. The minus sign before angle $\phi_i^{(2)}$ is required since gear rotation is considered negative in clockwise direction and $\phi_i^{(2)}$ makes the gear to move away from the pinion.

2. Nodal rotations $\theta_i^{(P1)}$ and $\theta_i^{(W1)}$ at reference nodes $P1$ and $W1$ (see Fig. 8) are obtained at each

contact position i from FEA. Rotation $\theta_i^{(P1)}$ results positive when pinion rotates in counterclockwise direction whereas rotation $\theta_i^{(W1)}$ results negative when gear rotates in clockwise direction.

3. Rotation $\theta_i^{(P1)}$ represents the pinion rotation due to tooth contact and bending deformations. To account for all these deformations in the determination of the transmission error, $-\theta_i^{(P1)} \cdot N_1/N_2$ will represent the rotation of the gear towards the pinion due to deformations. The minus sign is required to make it negative, since the deformations make the gear to move closer to the pinion. On the other hand, rotation $\theta_i^{(W1)}$ is set for each contact position by the user as $\theta_i^{(W1)} = \phi_i^{(2)}$.

4. The loaded transmission error is obtained as a discrete function as

$$\Delta\phi_i^{(l)} = \left(-\theta_i^{(W1)} - \theta_i^{(P1)}\frac{N_1}{N_2} \right) \tag{8}$$

5. Finally, the total function of transmission errors is obtained as

$$\Delta\phi_i = \Delta\phi_i^{(u)} + \Delta\phi_i^{(l)} \tag{9}$$

   where the peak-to-peak transmission error is defined as $\Delta\phi_{max} = \max(\Delta\phi_i) - \min(\Delta\phi_i)$.

5 Numerical results

5.1 Definition of examples of design

Eight examples of design of cylindrical parallel-axis gear drives have been defined. The common basic geometric design data are shown in Table 1.

For simplification reasons, all design examples have been organized into two groups:

- The first group consists of 4 examples comprising two examples of spur gear drives ($\beta_p = 0°$) and two examples of helical gear drives ($\beta_p = 20°$) generated by rack-cutter and grinding disk. For helical gear drives, a right hand pinion and a left hand wheel are considered. The particular design parameters for each example of design are shown in Table 2.

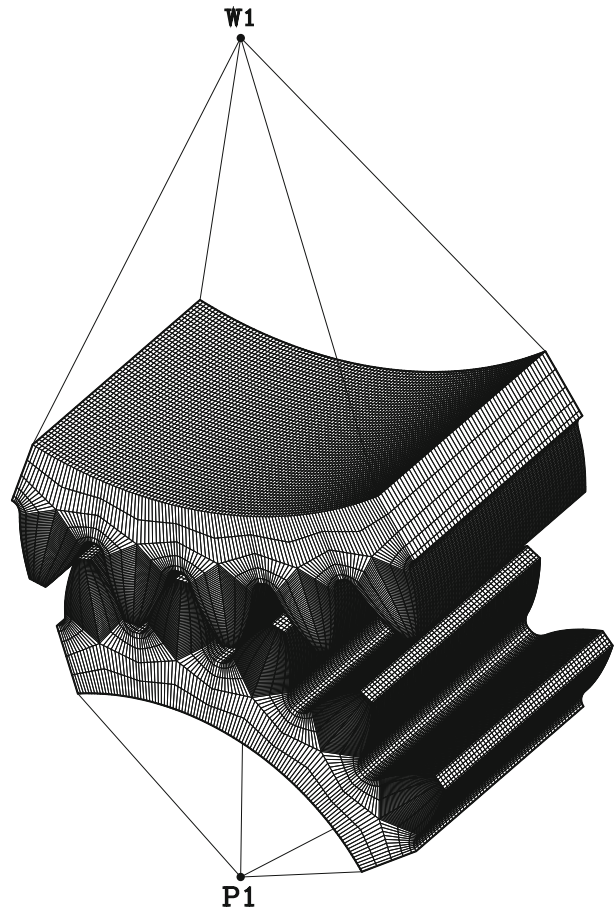**Fig. 8** Finite element model of a cylindrical gear drive for stress analysis

Table 1 Common basic design data of the investigated cylindrical parallel-axis gear drives

Parameter	PINION	WHEEL
Number of teeth, N	24	34
Module, m (mm)	2	
Face width, F_W (mm)	20	
Normal pressure angle, α_n (°)	25	
Edge radius coefficient, ρ	0.25	
Young's Modulus, E (GPa)	210	
Poisson's ratio, v	0.3	
Nominal torque applied, T (Nm)	150	–

- The second group consists of 4 examples of curvilinear gear drives generated by face-milling cutters ($r_c = 100$ mm). The particular design parameters for each example of design are shown in Table 3.

Table 2 Examples of design of spur and helical cylindrical gear drives

Example	β_p (°)	a_{pl} (1/mm)
1	0	0
2		0.000285
3	20	0
4		0.000275

All examples of design remain free of undercutting, interference, and pointing [9, 15]. Additionally, for those examples where point contact exists (examples 2, 4, 5 and 6), the corresponding plunging motion parabola coefficients a_{pl} and the cutter mean pitch curvature radii r_c have been selected in order to obtain a contact pattern where the contact ellipse located at its central part covers approximately 65% of face width F_W, as shown in Fig. 9.

Table 3 Examples of design of curvilinear cylindrical gear drives

Example	Type of curvilinear gear drive	Pinion drive surface
5	SBC	Concave
6		Convex
7	FSC	Concave
8		Convex

5.2 Optimal tip relief determination

An optimal tip relief modification, characterized by a combination of a parabola coefficient a_{tr} and a height h_{tr}, has been obtained for each of the design examples proposed in Sect. 5.1 under no misalignments and the applied pinion nominal torque shown in Table 1.

Table 4 shows the design parameters for the search of the optimal tip relief for all design cases. For each one, parameter h_{tr} has been maintained constant, whereas parameter a_{tr} has been increased gradually until the maximum contact stress throughout the whole cycle of meshing reaches its lowest value. Tip relief height h_{tr} has been chosen in such a way that never modifies the area of single tooth contact in cylindrical gear drives [10].

The application of tip relief to helical parallel-axis involute gear drives shows a significant effect on contact stresses, as it is illustrated in Fig. 10, basically because all lines of contact intersect the top edge of the gear tooth surfaces, causing high contact stresses all over the cycle of meshing. Figure 10 shows the evolution of contact and bending stresses along two cycles of meshing when parabola coefficient a_{tr} is increased for the example 3 (see Table 2). According to Fig. 10, the higher the parabola coefficient a_{tr} is, the higher the maximum bending stress will be because of

Table 4 Numerical simulation examples employed in load transfer optimization processes

| h_{tr} (mm)	0.7					
a_{tr} (1/mm)	0.00	0.01	0.02	0.03	0.04	0.05

the reduction of effective contact ratio, as mentioned in Sect. 2.5.

Figure 11 shows the effect of tip relief on contact stresses for the example of design 3 (helical gears with line contact). A higher value of Mises stresses is obtained when no tip relief is applied (Fig. 11a). Figure 11b shows a lower value of Mises stresses when a tip relief with parabola coefficient $a_{tr} = 0.03$ mm^{-1} and height $h_{tr} = 0.7$ mm is applied.

Finally, Table 5 shows the optimal tip relief parabola coefficients for each example of design shown in Tables 2 and 3. All the aforementioned coefficients have been applied prior to starting the analyses of the cylindrical gear drives.

5.3 Comparison of spur, helical and curvilinear gear drives designed for line contact

Examples of design 1, 3, 7 and 8 are considered in this section. The evolution of the maximum equivalent Von Mises contact and bending stresses along two

(a)   **(b)**   **(c)**
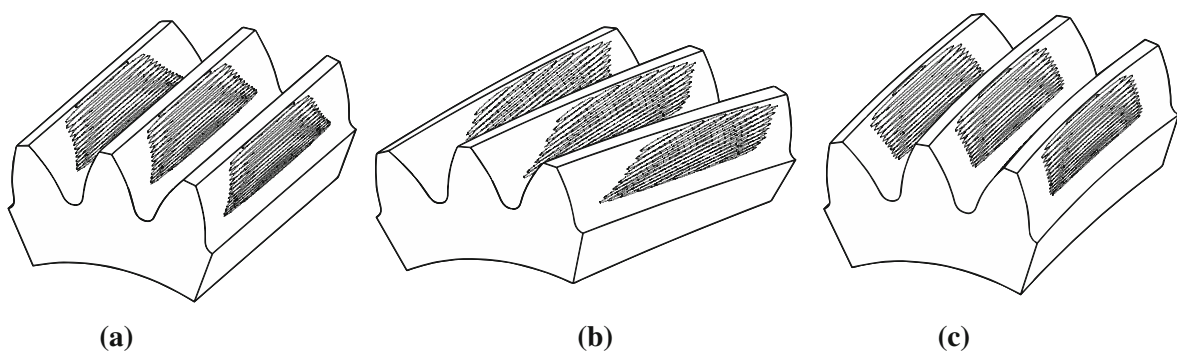
Fig. 9 Contact patterns corresponding to: **a** example 2, **b** example 4, and **c** example 5
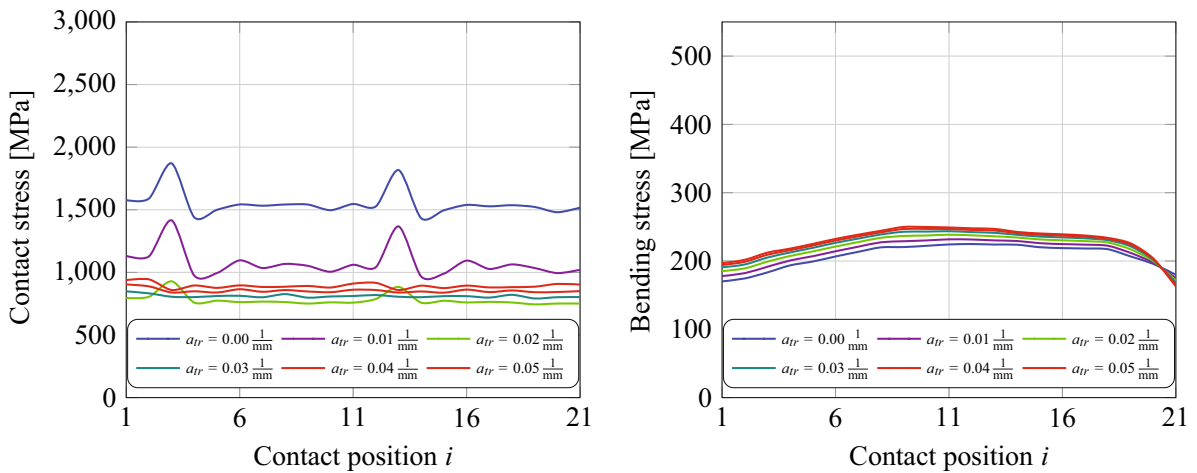
Fig. 10 Evolution of contact stresses (*left*) and bending stresses (*right*) for case of design 3
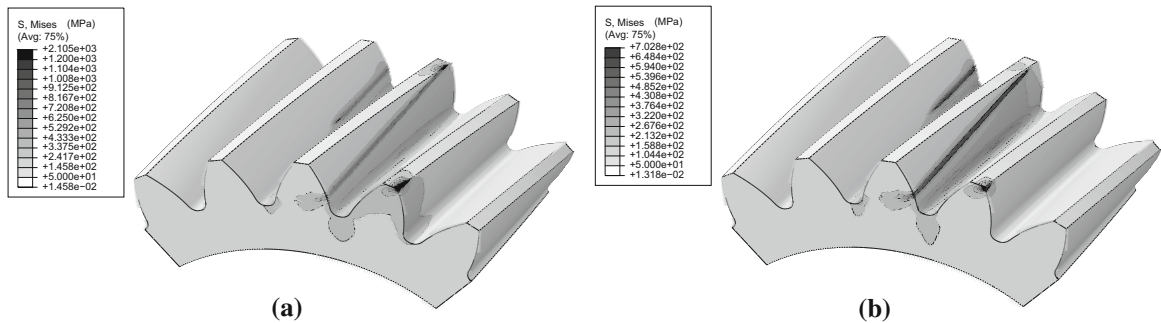

Fig. 11 Mises stresses on the pinion model for the example 3 of design in case of: **a** no tip relief, **b** a tip relief with $a_{tr} = 0.03$ mm^{-1} and $h_{tr} = 0.7$ mm

Table 5 Optimal tip relief parabola coefficients for all cases of design shown in Tables 2 and 3

Example	1	2	3	4	5	6	7	8
$(a_{tr})_{opt}$ (1/mm)	0.01	0.02	0.03	0.03	0.03	0.02	0.03	0.04

cycles of meshing on the pinion driving active surfaces has been investigated considering ideal conditions of assembly and two levels of crossing shaft angle error: $0.05°$ and $0.10°$. The crossing shaft angle error is the most representative error in parallel-axes cylindrical gears due to shaft deflections, as it is shown in [12].

Figure 12 shows the evolution of both contact and bending stresses for the gear drives designed for line contact under ideal assembly conditions. Spur and curvilinear gear drives show similar tendencies. The maximum contact and bending stresses in the helical

gear drive are the lowest due to the effect of the overlap ratio.

Figure 13 represents the evolution of both contact and bending stresses for cylindrical gear drives designed for line contact when a crossing shaft angle error of $\Delta H = 0.05°$ is present. As expected, the mean component of both contact and bending stresses has been increased in all the examples. The helical gear drive constitutes the most advantageous example under this angular misalignment condition, since it yields the lowest level of mean contact stress. Contact
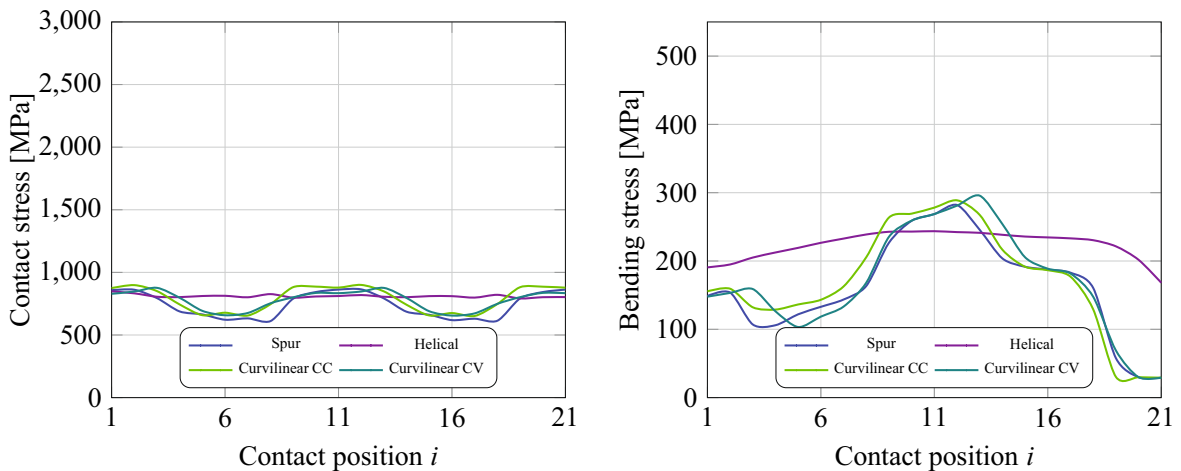
Fig. 12 Evolution of contact stresses (*left*) and bending stresses (*right*) for cylindrical gear drives designed for line contact under ideal assembly conditions
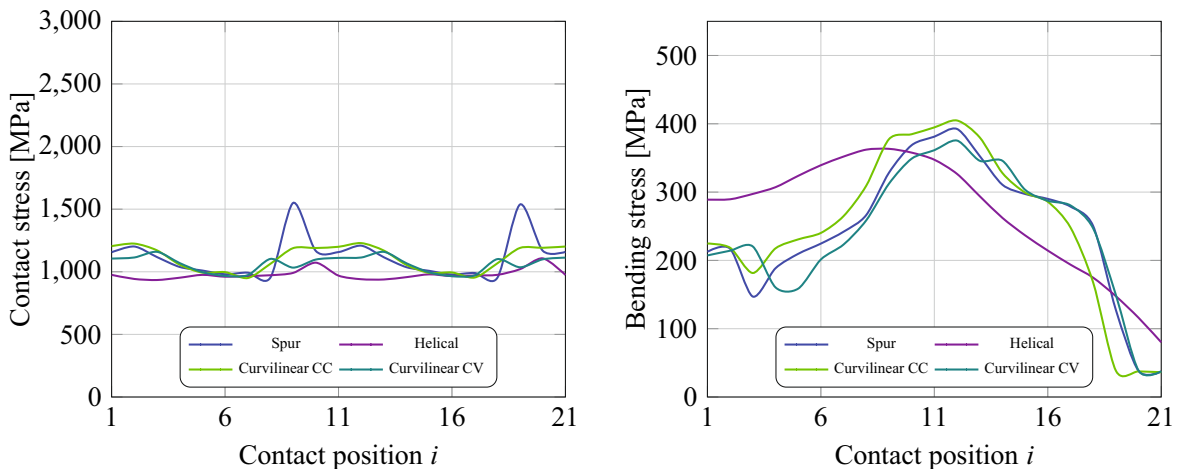

Fig. 13 Evolution of contact stresses (*left*) and bending stresses (*right*) for cylindrical gear drives designed for line contact when a crossing shaft angle error $\Delta H = 0.05°$ is present

stresses are slightly higher when the pinion concave active surfaces work as driving surfaces for curvilinear gears. Additionally, the spur gear drive presents areas of severe contact stresses due to edge contact.

Figure 14 shows the evolution of both contact and bending stresses for cylindrical gear drives designed for line contact when a crossing shaft angle error $\Delta H = 0.10°$ is present. Basically, the same tendencies are observed as in Fig. 13. However, the mean component of both contact and bending stresses is higher in all the examples and the edge contact phenomenon is more severe in the spur gear drive.

5.4 Comparison of spur, helical and curvilinear gear drives designed for point contact

Examples of design 2, 4, 5 and 6 are considered in this section. Figure 15 illustrates the evolution of both contact and bending stresses for cylindrical gear drives designed for point contact under ideal assembly conditions. As expected, both contact and bending stresses have increased with respect to Fig. 12 due to localization of the bearing contact. All examples of design yield similar mean contact and bending stresses, whereas the helical gear drive provides the
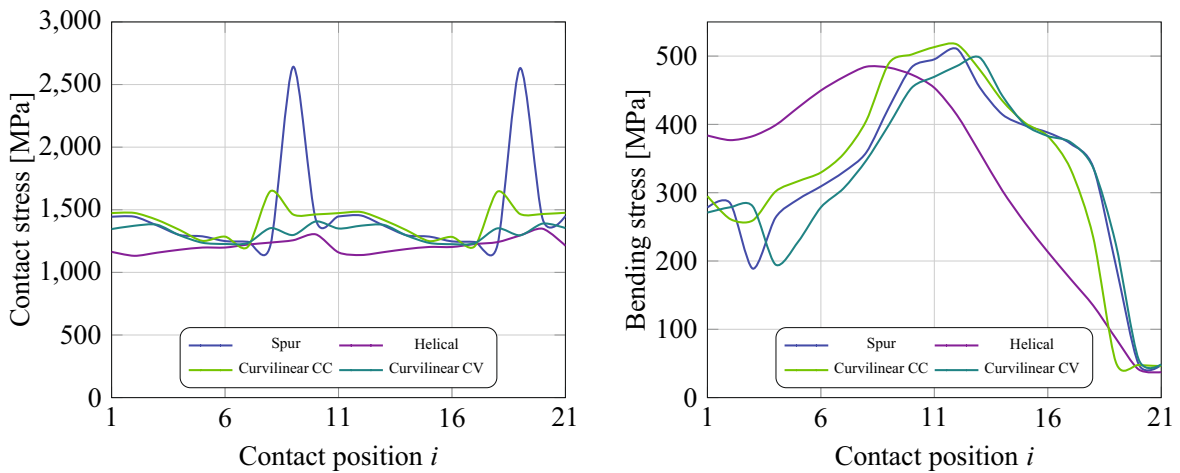
Fig. 14 Evolution of contact stresses (*left*) and bending stresses (*right*) for cylindrical gear drives designed for line contact when a crossing shaft angle error $\Delta H = 0.10°$ is present
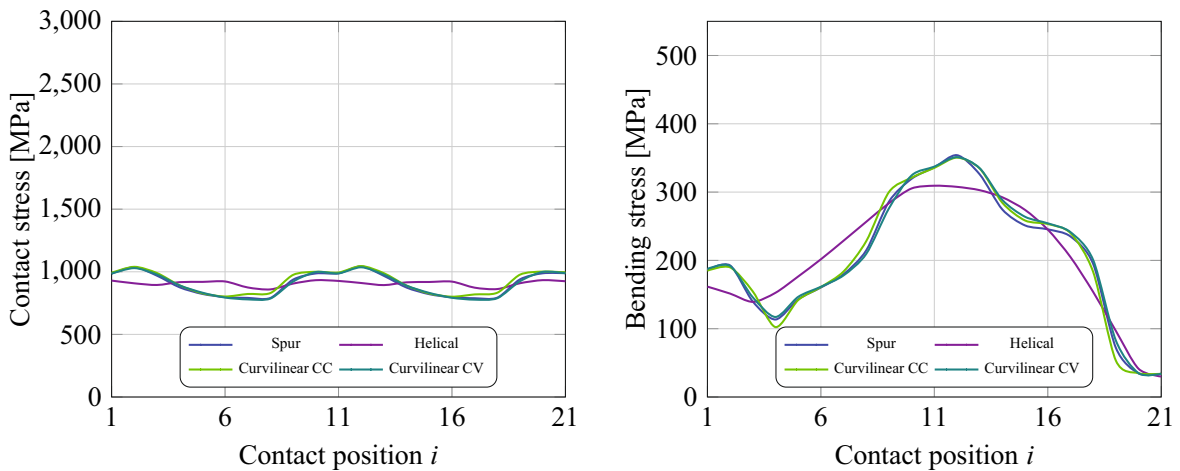

Fig. 15 Evolution of contact stresses (*left*) and bending stresses (*right*) for cylindrical gear drives designed for point contact under ideal assembly conditions

lowest alternating components of both mechanical variables because of the helix contact ratio.

Figure 16 represents the evolution of both contact and bending stresses for cylindrical gear drives designed for point contact when a crossing shaft angle error $\Delta H = 0.05°$ is present. Both spur and curvilinear gear drives yield mean contact and bending stresses lower than the corresponding to the helical gear drive. Areas of severe contact stresses appear when pinion convex active surfaces work as driving surfaces at curvilinear gear drives.

Figure 17 shows the evolution of both contact and bending stresses for cylindrical gear drives designed for point contact when a crossing shaft angle error

$\Delta H = 0.10°$ is present. The same tendencies are observed as in Fig. 16.

The obtained results show a better mechanical behavior in cylindrical gear drives designed for point contact respect to those designed for linear contact when severe shaft angle error is present.

5.5 Comparison of spur, helical and curvilinear gear drives designed for only one generating process

Examples of design 1, 3, 5 and 6 are considered in this section. Figures 18, 19 and 20 illustrate the evolution of the maximum equivalent Von Mises contact and
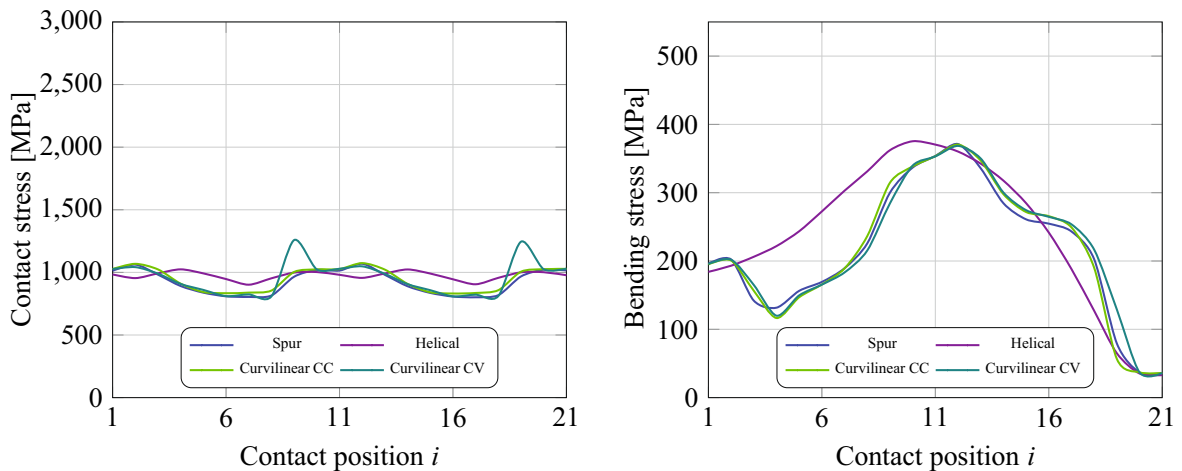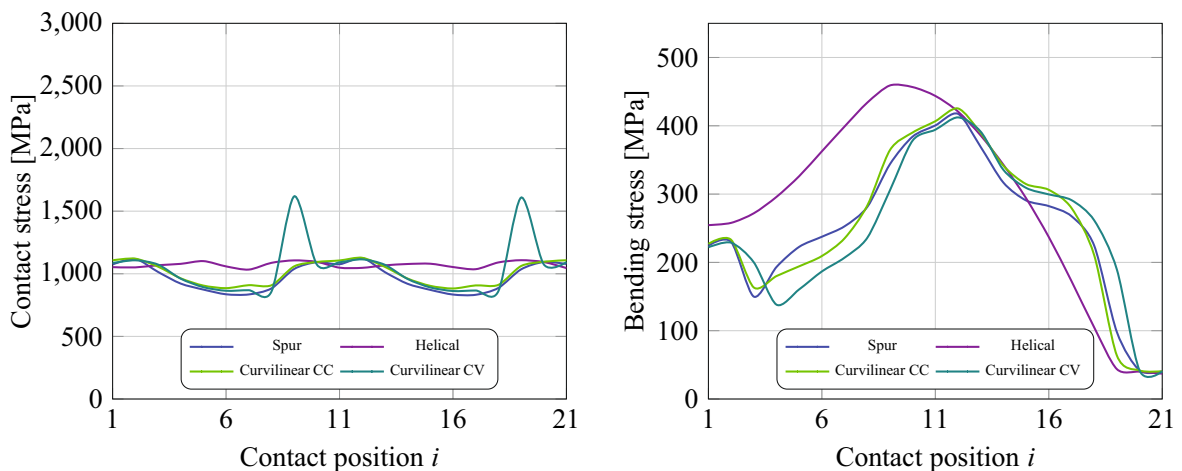
Fig. 16 Evolution of contact stresses (*left*) and bending stresses (*right*) for cylindrical gear drives designed for point contact when a crossing shaft angle error $\Delta H = 0.05°$ is present

Fig. 17 Evolution of contact stresses (*left*) and bending stresses (*right*) for cylindrical gear drives designed for point contact when a crossing shaft angle error $\Delta H = 0.10°$ is present

bending stresses along two cycles of meshing on the pinion driving active surface for the mentioned examples under ideal assembly conditions and when shaft angle error is present. Based on the obtained numerical results the following remarks can be made:

- Under no misalignments, both spur and helical gear drives present the lowest mean contact and bending stresses respect to curvilinear gear drives due to the advantages of line contact respect to point contact.
- If angular misalignments between gear supporting shafts appear, the mean contact and bending stresses corresponding to spur and helical gear

drives increase substantially, whereas the corresponding to *SBC-type* curvilinear gear drives increase barely, just as mentioned previously in Sect. 5.4. The greater the crossing shaft angle error ΔH is, the higher the differences between them will be. Under moderate angular misalignments ($\Delta H = 0.05°$), *SBC-type* curvilinear gear drives yield a slightly lower mean contact stress than the corresponding to spur and helical gear drives, while under severe angular misalignments ($\Delta H = 0.10°$), the great benefit of replacing spur and helical gear drives by *SBC-type* curvilinear gear drives is obvious.
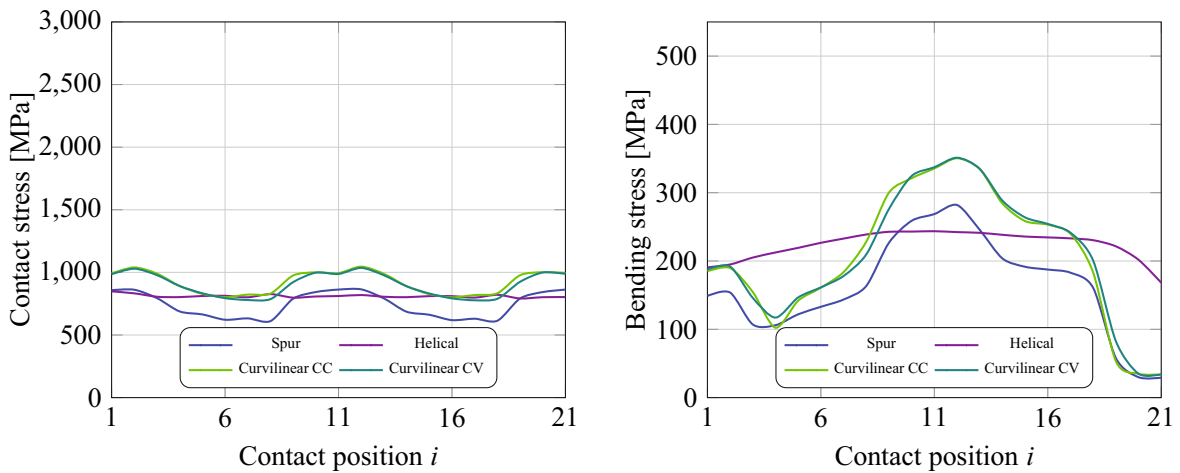
Fig. 18 Evolution of contact stresses (*left*) and bending stresses (*right*) for cylindrical gear drives generated with only one cutting process and no misalignments
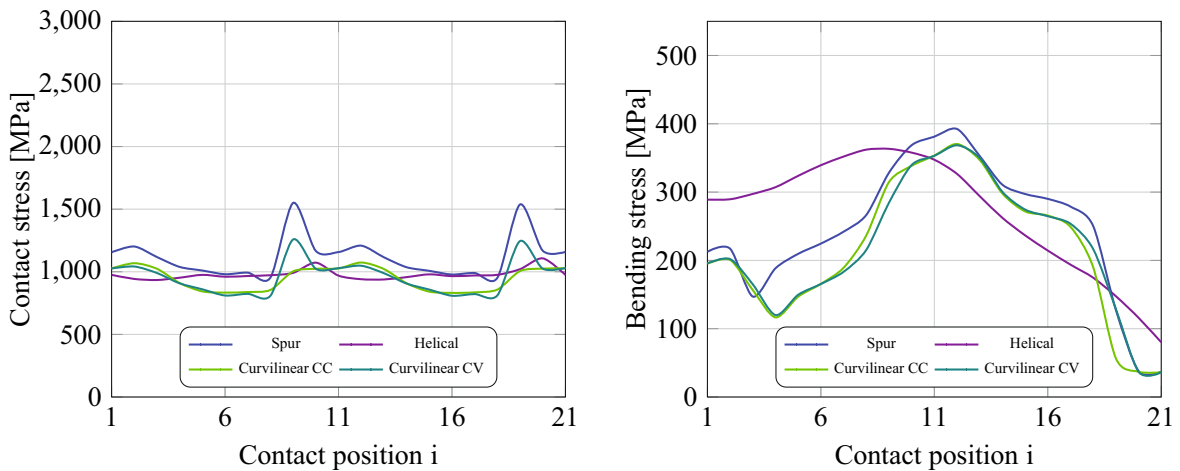

Fig. 19 Evolution of contact stresses (*left*) and bending stresses (*right*) for cylindrical gear drives generated with only one cutting process when a crossing shaft angle error $\Delta H = 0.05°$ is present

- Edge contact phenomenon takes places in *SBC-type* curvilinear gear drives when pinion convex active surfaces work as driving surfaces under any degree of angular misalignments.

5.6 Comparison of spur, helical and curvilinear gear drives considering transmission errors

Unloaded function of transmission errors, loaded function of transmission errors, and total function of transmission errors, have been obtained for each example of design under ideal assembly conditions

and under crossing shaft angle errors of 0.05° and 0.10°. Figure 21 (left) shows the three mentioned functions for example 4 of design when a crossing shaft angle error of 0.05° is present. Here, a piece-wise linear function of unloaded transmission errors and a peak-to-peak value of 23.53 arcsec are observed.

Figure 21 (right) shows the evolution of the peak-to-peak value of the total function of transmission errors for those examples that have been designed for linear contact under ideal assembly conditions. It is observed that the peak-to-peak value of transmission errors increases with the crossing shaft angle error. The lowest values of transmission errors are reached in
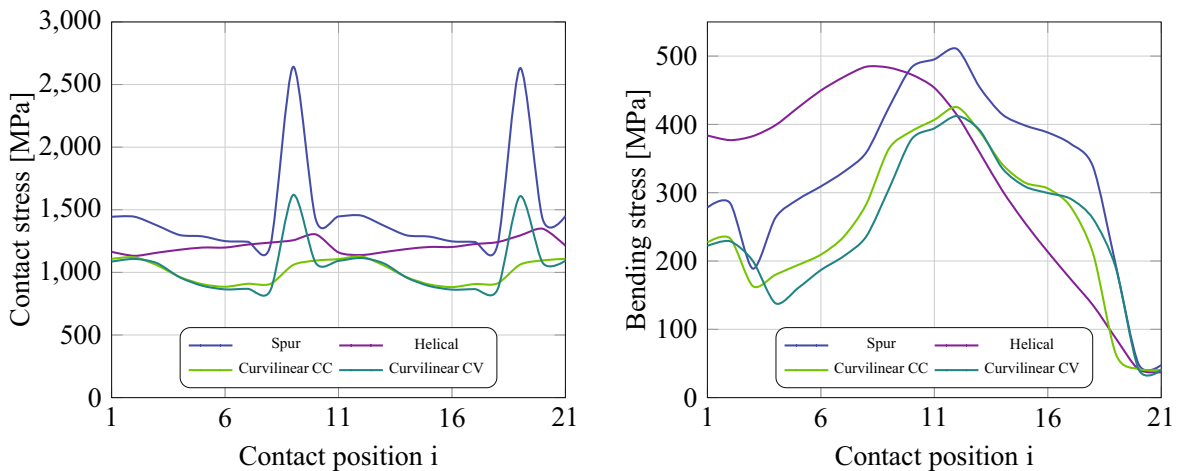
Fig. 20 Evolution of contact stresses (*left*) and bending stresses (*right*) for cylindrical gear drives generated with only one cutting process when a crossing shaft angle error $\Delta H = 0.10°$ is present
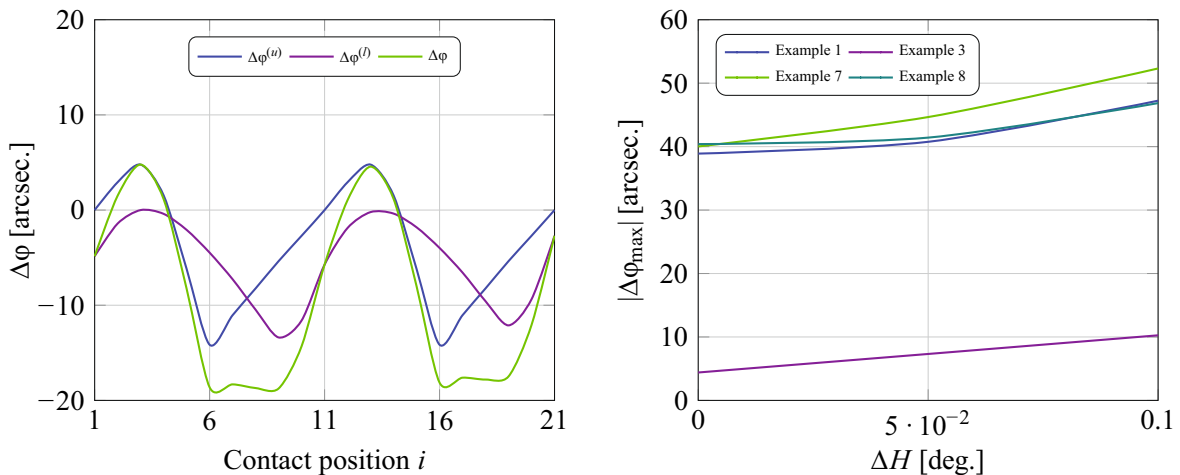

Fig. 21 Example of unloaded, loaded and total functions of transmission errors (*left*) for example 4 of design with $\Delta H = 0.05°$, and evolution of peak-to-peak transmission error

for cylindrical gear drives designed for line contact under different assembly conditions (*right*)

helical gear drives. Similar results are obtained in curvilinear and spur gear drives.

Figure 22 (left) shows the evolution of the peak-to-peak value of the total function of transmission errors for those examples that have been designed for point contact under ideal assembly conditions. The lowest values are obtained in helical gear drives whereas the highest values are obtained in spur gear drives.

Figure 22 (right) shows the evolution of the peak-to-peak value of the total function of transmission errors for those examples that have been designed for

only a generating process. The lowest values are obtained in helical gear drives whereas the highest values are obtained in curvilinear gear drives.

6 Conclusions

Based on the conducted research work, the following conclusions can be drawn:

1. Application of optimal tip relief to gear tooth surfaces improves the endurance of spur, helical and curvilinear gear drives, especially in helical
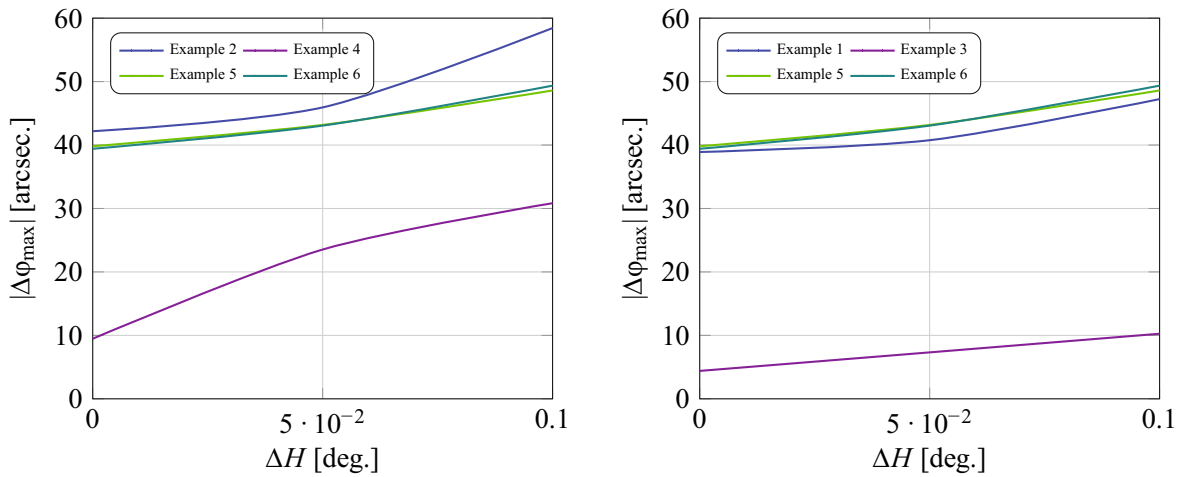
Fig. 22 Evolution of peak-to-peak transmission error for cylindrical gear drives designed for point contact (*left*) and generated through simple generating processes (*right*) under different assembly conditions

gear sets, by reducing the maximum contact stresses on the gear tooth surfaces.

2. *FSC-type* curvilinear gear drives do not provide meaningful advantages compared to helical gear drives with line contact.

3. Application of *SBC-type* curvilinear gear drives with localized bearing contact, instead of conventional involute spur or helical gear drives, is justified in presence of severe angular misalignments considering the obtained contact stresses. However, from the point view of the peak-to-peak values of transmission errors, helical gears constitute the best solution.

4. From the mechanical behavior point of view, curvilinear gear drives work better when pinion concave active surfaces operate as driving surfaces in presence of angular misalignments.

5. The application of profile crowning in order to predesign a parabolic function of transmission errors in curvilinear and spur gear drives might be advisable, basically due to the high maximum levels of loaded transmission errors reached in both of them under non-ideal assembly conditions.

References

1. ABAQUS/Standard User's Manual (2010) Providence, Rhode Island 02909-2499 (US)
2. Andrei L, Andrei G, Epureanu A, Oancea N, Walton D (2002) Numerical simulation and generation of curved face width gears. Int J Mach Tools Manuf 42(1):1–6
3. Arafa HA (2005) C-gears: geometry and machining. Proc Inst Mech Eng C J Mech Eng Sci 219(7):709–726
4. Arafa HA, Bedewy M (2010) C-gears in rotorcraft transmissions: a novel design paradigm. In: International powered lift conference 2010, pp 93–100
5. Arafa HA, Bedewy M (2010) Quasi-exact-constraint design of wind turbine gearing. In: American society of mechanical engineers, power division (publication) POWER, pp 607–616
6. Arafa HA, Bedewy M (2012) Manufacturability and viability of different c-gear types: a comparative study. In: Proceedings of the ASME design engineering technical conference vol 5, pp 381–391
7. Artoni A, Bracci A, Gabiccini M, Guiggiani M (2009) Optimization of the loaded contact pattern in hypoid gears by automatic topography modification. J Mech Des Trans ASME 131(1):011,008
8. Bracci A, Gabiccini M, Artoni A, Guiggiani M (2009) Geometric contact pattern estimation for gear drives. Comput Methods Appl Mech Eng 198(17–20):1563–1571
9. Budynas RG, Nisbett JK (2014) Shigley's mechanical engineering design, 10th edn. McGraw-Hill Education, New York
10. Fuentes A, Gonzalez-Perez I, Sanchez-Marin FT, Hayasaka K (2012) On the behaviour of asymmetric cylindrical gears in gear transmissions. In: Proceedings of FISITA 2012 world automotive congress, lecture notes in electrical engineering, vol 193, pp 143–150
11. Fuentes A, Ruiz-Orzaez R, Gonzalez-Perez I (2014) Computerized design, simulation of meshing, and finite element

analysis of two types of geometry of curvilinear cylindrical gears. Comput Methods Appl Mech Eng 272:321–339

12. Gonzalez-Perez I, Roda-Casanova V, Fuentes A (2015) Modified geometry of spur gear drives for compensation of shaft deflections. Meccanica 50(7):1855–1867

13. International Organization for Standardization: ISO 1122-1:1998 (1999) International standard. Vocabulary of gear terms—part 1: definitions related to geometry. Technical corrigendum 1

14. International Organization for Standardization: BS ISO 21771:2007 (2007) International standard. Gears—sylindrical involute gears and gear pairs: concepts and geometry

15. Litvin FL, Fuentes A (2004) Gear geometry and applied theory, 2nd edn. Cambridge University Press, Cambridge

16. Litvin FL, Fuentes A, Gonzalez-Perez I, Carvenali L, Kawasaki K, Handschuh RF (2003) Modified involute helical gears: computerized design, simulation of meshing and stress analysis. Comput Methods Appl Mech Eng 192(33–34):3619–3655

17. Parshin A (2014) Arched toothed cylindrical gears manufacture on CNC lathes and experience of their inculcation. In: Proceedings of the international symposium theory and practice of gearing, pp 151–159

18. Parsons BN, Walton D, Andrei L, Andrei G (2004) Nonstandard cylindrical gears. Gear Technol 21(6):30–37

19. Radzevich SP (2012) Dudley's handbook of practical gear design and manufacture, 2nd edn. CRC Press, Boca Raton

20. Sheveleva GI, Volkov AE, Medvedev VI (2007) Algorithms for analysis of meshing and contact of spiral bevel gears. Mech Mach Theory 42(2):198–215

21. Shue-Tseng L (1988) Curvilinear cylindrical gears. Gear Technol 5(3):8–12

22. Tseng RT, Tsay CB (2001) Mathematical model and undercutting of cylindrical gears with curvilinear shaped teeth. Mech Mach Theory 36(11–12):1189–1202

23. Tseng RT, Tsay CB (2004) Contact characteristics of cylindrical gears with curvilinear shaped teeth. Mech Mach Theory 39(9):905–919

24. Tseng JT, Tsay CB (2005) Mathematical model and surface deviation of cylindrical gears with curvilinear shaped teeth cut by a hob cutter. J Mech Des Trans ASME 127(5):982–987

25. Tseng JT, Tsay CB (2006) Undercutting and contact characteristics of cylindrical gears with curvilinear shaped teeth generated by hobbing. J Mech Des Trans ASME 128(3):634–643

26. Wu YC, Chen KY, Tsay CB, Ariga Y (2009) Contact characteristics of circular-arc curvilinear tooth gear drives. J Mech Des Trans ASME 131(8):081,003